

RAPID VARIABILITY OF BLAZARS

MARCO CHIABERGE¹, GABRIELE GHISELLINI²

¹ *S.I.S.S.A., via Beirut 2-4, 34014 Trieste, Italy*

² *Osservatorio Astronomico di Brera, Via Bianchi 46, 22055 Merate, Italy*

ABSTRACT. Blazars are characterized by large amplitude and fast variability, indicating that the electron distribution is rapidly changing, often on time scales shorter than the light crossing time. We study the time dependent behavior of the electron distribution after episodic electron injection phases, and calculate the observed synchrotron and self Compton radiation spectra. Since photons produced in different part of the source have different travel times, the observed spectrum is produced by the electron distribution at different stages of evolution. Time delays between the light curves of fluxes at different frequencies are possible, as illustrated for the specific case of the BL Lac object Mkn 421.

1. Introduction

Variability is one of the defining properties of blazars, characterized by variations of their flux even of two orders of magnitude in time scales of years, and smaller changes, but still up to factor 2, in hours/days time scales. Light curves as seen, e.g., in the X-rays and in the optical, often show a quasi-symmetric behavior, with rise and decay time scales approximately equal (see i.e. Urry et al. 1997, Ghisellini et al. 1997, Massaro et al. 1996, Giommi et al. 1998), indicating that both times are connected to the light travel time across the source R/c , and therefore suggesting that the cooling times of the emitting electrons are shorter. Furthermore this implies that the emitting electron distribution is significantly changing on time scales shorter than R/c , at least at these energies. In order to reproduce the observed variability pattern we need to study the time evolution of the emitting particles distribution *and* to take into account the different light travel times of photons produced in different regions of the source. The observed flux is then, at any time, *the sum of the emission produced by particle distributions of different ages*, each one produced in a different region of the source: even a homogeneous source then resembles an inhomogeneous one. In §2 we shortly present the model assumptions, in §3 we show some results of the simulations in the case of electron distributions homogeneously injected throughout the source and in a more realistic case of a shock traveling down a region of a jet. In §4 we apply our model to the specific case of MKN 421.

2. The model

We assume that the emission is produced by a distribution of relativistic electrons injected in a region of typical dimension R embedded in a tangled magnetic field B , at a rate $Q(\gamma)$ [$\text{cm}^{-3} \text{s}^{-1}$] (γ is the electrons Lorentz factor). Electrons lose energy by

emitting synchrotron and synchrotron self-Compton radiation (SSC). Escape from the source is also considered (t_{esc} is assumed being independent of energy). The continuity equation governing the temporal evolution of the electron distribution $N(\gamma, t)$ [cm^{-3}] is

$$\frac{\partial N(\gamma, t)}{\partial t} = \frac{\partial}{\partial \gamma} [\dot{\gamma}(\gamma, t)N(\gamma, t)] + Q(\gamma, t) - \frac{N(\gamma, t)}{t_{esc}} \quad (1)$$

where $\dot{\gamma} = \dot{\gamma}_S + \dot{\gamma}_C$ is the total cooling rate (synchrotron and synchrotron self-Compton). We calculate SSC spectra produced by the calculated electrons distribution at any given time. The details of the numerical method used to solve the equation are illustrated in Chiaberge & Ghisellini (1998). If the particle distribution evolves more rapidly than R/c the observer will see, at any time, a convolution of different spectra, each produced in a different part of the source. Initially the observer only sees the emission coming from fresh electrons located in the region ('slice') closest to her/him; then the inner parts of the source become visible, also showing 'young' spectra, while electrons in the front slices are evolving. After a time R/c all the emitting region will be visible: the back of it with fresh electrons and the front of it with older electrons. In order to take into account this effect, we divide the source of size R into n slices of equal thickness $R_{sl} < t_{min}$ (t_{min} is the shorter among cooling, injection and escape times). In this way, each single slice can be considered as an homogeneous emitting region. We then sum the contribution of each slice at any time. We consider slices having equal volumes (assuming a 'cubic' geometry), with the line of sight placed at 90° with respect to one face of the cube. This angle, in the lab frame, transforms to a viewing angle of $\sim 1/\Gamma$, if the source moves with a Lorentz factor Γ , which is appropriate for blazars. Extension to different geometries (i.e. cylinder, sphere, etc) is trivial, by properly weighting each slice volume and does not affect the results. Even in the simplest 'cubic' case time-lags among light curves at different frequencies are observable.

3. Discussion

We summarize here the results of the simulations of two different illustrative injection phases: i) narrow Gaussian electron distribution centered at $\gamma = 10^5$ lasting for a time $t_{inj} \ll R/c$; ii) power law electron distribution ($Q(\gamma) \propto \gamma^{-p}$, $p = 1.7$) between $\gamma_{min} = 1$ and $\gamma_{max} = 10^5$, lasting for a time $t_{inj} = R/c$. The source physical parameters are: $R = 10^{16}$ cm, $B = 1$ Gauss, injected luminosity $L_{inj} = 4 \times 10^{41}$ erg s $^{-1}$, $t_{esc} = 1.5R/c$. We stress that our main purpose is to reproduce the quasi-symmetric light curves often observed at optical-X rays frequencies, in order to put strict constraints on the physical parameters of a source producing such a variability pattern. The main difference between injecting a Gaussian distribution of electrons and injecting a power-law (with $p > 0$) is that in the first case the emission will be concentrated first at high frequencies, and only after some t_{cool} electrons can substantially emit at lower frequencies. This produces a time delay between the peaks of the emission at different frequencies in case (i) (see fig. 1). Also notice the different behavior of the light curves at different frequencies, showing plateau at the highest corresponding electron energies. In case (ii) at frequencies where $t_{cool} \ll R/c$ both the rise and the decay are controlled by the light crossing time, and we have symmetric light curves with time lags depending on the different cooling times.

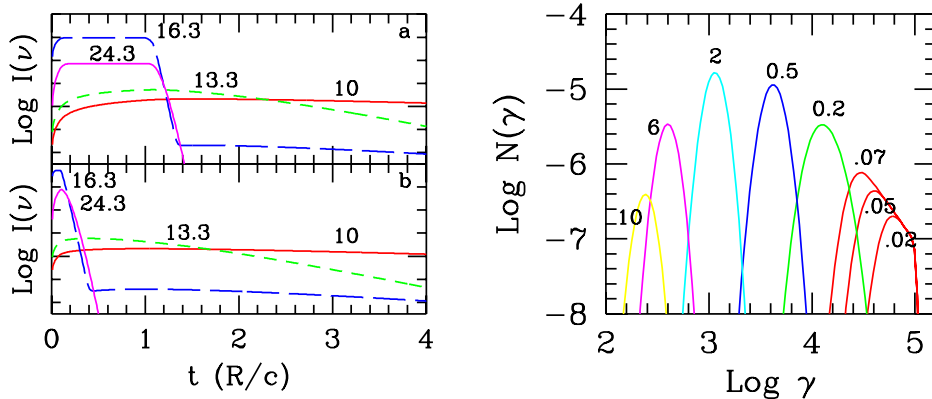


Fig. 1. *Left*: light curves of the specific intensity at different frequencies, as observed in the comoving frame, in the case of Gaussian injection and $t_{inj} \ll R/c$, to illustrate light crossing time effects, included in a) and ignored in b). Labels correspond to the logarithm of the frequency. For clarity, the intensity of each light curve has been multiplied by different constants. *Right*: time evolution of the particle distribution $N(\gamma)$ corresponding to an injection of particles distributed in energy as a Gaussian, centered at $\gamma = 10^5$, for $t_{inj} = 0.1R/c$. Labels indicate time after the beginning of the injection, in units of R/c .

According to our results, quasi symmetric light curves can be only originated in two cases: 1) $t_{inj} \ll R/c \sim t_{cool}$; 2) $t_{inj} \sim R/c$ and $t_{cool} \ll R/c$. In case (1) symmetric light curves are present only within a very small range of frequencies ($t_{cool} \sim R/c$), while in case (2) quasi-symmetric light curves can occur at all frequencies corresponding to particle cooling time scales shorter than R/c . Furthermore the second case can be interpreted as a result of a shock lasting for a time $t_{inj} \sim R/c$. In fact, we reproduced the case of a shock of longitudinal dimension R and width $r_s \ll R$ running along a region of the jet of same dimension R (perpendicular to the jet axis). As in the previous cases, we assume that the observer is located at an angle $1/\Gamma = \sqrt{1 - \beta^2}$ from the jet axis, such that the viewing angle in the comoving frame is 90° . We calculate the observed light curves in the comoving frame, by summing the contributions of each part of the source, taking into account both the traveling of the shock across the source (accelerating particles in different regions at different times, as the shock travels across the source) and the light travel time effect. Details are presented in Chiaberge & Ghisellini (1998). The light curves obtained in this shock case are similar to the corresponding ‘homogeneous’ case ($t_{inj} = R/c$), with slightly longer time-lags (see fig. 2)

4. Application to MKN 421

In May 1994 the ASCA satellite revealed an X-ray flare of the nearby ($z = 0.03$) BL Lac object (Takahashi et al. 1996) during an high state of TeV emission (Macomb et al. 1995). Observations report an increase of a factor ~ 2 of the 2–10 keV flux, with a doubling time scale of ~ 12 hours. Much less amplitude variability is present in the

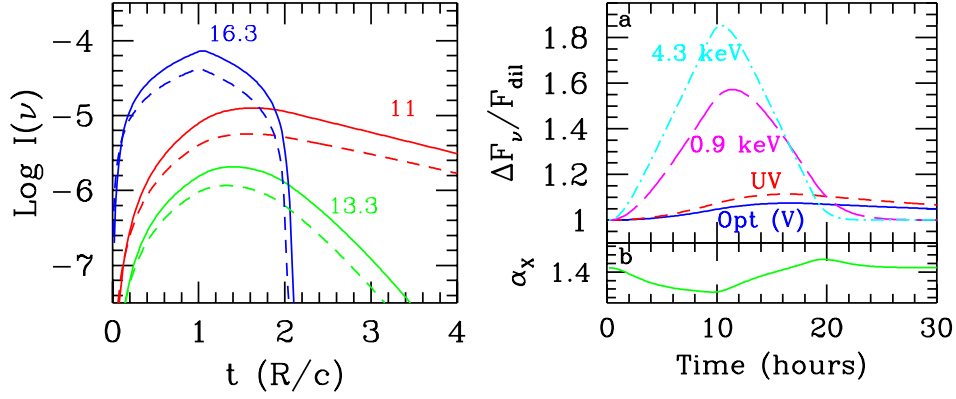


Fig. 2. *Left*: simulated light curves at different frequencies in the case of power law injection lasting for a time $t_{inj} = R/c$ (dashed lines, homogeneous injection case) and in the case of a shock active for a time $t = R/c$ traveling across a region of dimension R (solid lines). *Right*: simulated light curves at different frequencies (a) and X-ray spectral index (b) for the Mkn 421 May 1994 flare.

IR, optical, UV and GeV bands. Takahashi et al. (1996) found a time-lag between hard X-rays (2 – 7.5 keV) and soft X-rays (0.5 – 1.5 keV) of ~ 1 hour: the hard X-rays lead the soft X-rays. They interpret this as due to synchrotron cooling. We can qualitatively reproduce this behavior, assuming that the rapid variability is due to the sum of a rapidly evolving component and a quasi-constant one, corresponding to the high state fit of the spectral energy distribution (Chiaberge & Ghisellini, 1998). We take into account the effects of beaming using the following transformations: if Γ is the bulk Lorentz factor, θ the viewing angle and $\delta = [\Gamma(1 - \beta \cos \theta)]^{-1}$ the beaming factor, the observed intensity is $I(\nu) = \delta^3 I'(\nu')$ and $t = t'/\delta$, where $I'(\nu')$ and t' are the comoving intensity and comoving time scales, respectively. We found the following parameters for the variable component: $R = 1.5 \times 10^{16}$ cm, $B = 0.13$ Gauss, $\delta = 15.5$, $\ell_{inj} = 1.5 \times 10^{-3}$, $Q(\gamma) \propto \gamma^{1.4} \exp(-\gamma/\gamma_{max})$ between $\gamma_{min} = 10^3$ and $\gamma_{max} = 8.5 \times 10^5$. We perform the simulation in the shock case with $r_s = 0.1R/c$ (width of the shock), $t_s = R/c$ (time during which the shock is active) and $\beta'_s \sim 1$ (velocity of the shock in the comoving frame). Light curves and X-ray spectral index variability are reported in fig 2.

References

- Chiaberge, M. Ghisellini, G.: 1998, M.N.R.A.S., submitted.
 Ghisellini, G. et al., 1997: *Astron. Astrophys.* **327**, 61.
 Giommi, P. et al., 1998: *Astron. Astrophys. Lett.* **335**, LL5.
 Macomb, D.J. et al., 1995, ApJ, 449, L99
 Massaro, E. et al., 1996: *Astron. Astrophys.* **314**, 87.
 Takahashi, T. et al., 1996: *Astrophys. J. Lett.* **470**, LL89.
 Urry, C.M. et al., 1997: *Astrophys. J.* **486**, 799.